High Resolution X-ray Tomography for Stationary Multiphase Flows

D. Schmitz, N. Reinecke, G. Petritsch, D. Mewes

Institut für Verfahrenstechnik

Universität Hannover

Hannover

Germany

ABSTRACT

The high resolution which can be obtained by computer assisted tomography is used to investigate the liquid distribution and void fraction in random and structured packing. With a spatial resolution of 0.4×0.4mm² it is possible even to detect thin liquid films on structured packings. The experimental set-up consists of a custom-built second generation tomograph. The imaged object consists of a column filled with either a random ceramic packing of spheres or a structured metal packing. The liquid and void fraction distribution in random and structured packings with a quiescent gaseous phase is visualized. The water/air system is used. The liquid distributor consists of a perforated plate. The experimental hold-up values averaged over the column cross-section are in good agreement with empirical equations.

1 INTRODUCTION

In many chemical engineering applications random and structured packings are used to enhance the heat and mass transfer between two phases. These packings are used to obtain a high specific interfacial area to improve heat and mass transfer. They are in contact with co- and countercurrent flow of liquid and gas. As random packings spheres, cylinders or more complex bodies are used. They can consist of ceramic, polyolifiens, metal or carbon. The distribution of the packing elements inside the column is random. This also results in a random distribution of the void fraction, which influences the liquid distribution in the packing. Unlike the random packings structured packings offer a regular distribution of the void fraction. Because of this the liquid and gas flow in the packing is more homogeneous. The packings used can consist of folded metal.

Tomographic measurement techniques for process engineering applications have become increasingly popular. The aim of tomographic measurement is to get information on the distribution of the

physical properties inside the measurement plane. Originally X-ray tomography has been invented for medical purposes as described by Hounsfield [1]. The advantage of these techniques is the non-intrusiveness of the measurement inside the reactor. Lately, X-ray techniques have become more popular for usage with multiphase systems. Kantzas [2] and Lutran *et.al.* [3] are using a medical CT for the investigation of liquid distribution and holdups in trickle or fluidized beds. Toye *et.al.* [4] is using a custom built CT for investigations on the liquid distribution of random packing. Ikeda *et.al.* [5] discussed the problem of density fluctuation of two-phase flow on the reconstruction. He confirmed that multiphase systems with a quasi-stationary character can be imaged using this technique. Most of the CT-systems used for investigations on multi-phase flows are in their timeal resolution limited due to the energy of the penetrating photons observed for X-ray sources. Using CT- systems of the fourth generation (electron beam tomography) it is possible to achieve a time resolution in the order of 50 milliseconds. Peschman *et.al.* [6] describes such a system and discusses the applicability for technical use. Such a system offers a good time resolution even for unsteady flow conditions, but suffers from the low energy obtained from the x-ray generator.

2 X-RAY-TOMOGRAPHY

The actual tomographic measurement of any given property distribution can be subdivided into two individual processes. This is schematically shown in Figure 1. In Figure 1a the abstract measurement chain is depicted schematically. It consists of the measurement of the integral property and the calculation of the local property from the integral values. These different steps are also distinguishable from the true physical measurement chain depicted in Figure 1b. It consist of the sensor, the measurement device and the reconstruction. A good survey of technical aspects and reconstruction techniques is given by Ter-Pogssian *et.al* [7] as well as Herman [8]. The measurement process can be schematically described as shown in Figure 2. The tomographic measurement process requires the knowledge of some integral property of the unknown property distribution $f(x,y,z,t)$. This is generated by integrating the property distribution in the measurement plane along known paths s:

$$\Phi_M(\xi,\Theta,z,t) = \int_{s(\xi,\Theta,z)} f(x,y,z,t)d\vec{s} \,. \tag{1}$$

The obtained integral measurement value $\Phi_M(x,\Theta)$ is linearly independent if the linear and angular coordinates ξ and Θ, respectively, are different (Actually for the angular coordinate the limitation is

π but this is insignificant for the sake of the argument). Given a circular measurement plane which is convenient for most applications, the number of linearly independent measurements taken is given by the size of the discretization of the detector ξ and the number of views taken for different angles Θ.

X-ray Computed Tomography uses the interaction of high energetic radiation with matter as physical measurement principle. The radiation is weakened by the interaction with the matter. Weakening is dependent from the thickness d of the material and the linear attenuation coefficient μ. The linear attenuation coefficient itself is dependent on the energy of the radiation. The intensity of the weakened X-ray I is given by Beer's law:

$$I = I_0 \, e^{-\mu d} . \tag{2}$$

In equation (2) I_0 is the intensity of the non-weakened radiation. Equation (2) only applies to monochromatic radiation. For polychromatic radiation the dependence of the absorption coefficient on the radiation energy has to be considered. A complete set of integral measurement values for one angle is called a projection. For real tomographs the projections can be obtained in two different ways:

- the integral measurement values are sampled in a parallel beam geometry,
- the integral measurement values are sampled in a fan beam geometry.

For the reconstruction of tomographic images, the filtered backprojection is mostly employed. It is applicable for the reconstruction for full data problems where a sufficient number of projections are obtained. This technique is described by Brooks and di Chiro [9] as well as Kak and Slaney [10]. Backprojection can be thought of as reversing the data collection process. Each sample within a given projection represents the fractional transmittance of a narrow beam of X-rays through the object, which is assumed to be sufficiently well approximated by small, discrete pixels of constant attenuation. During backprojektion the value of each sample in the profile is numerically added to all of the image pixels, that participated in the attenuation process for that sample. Conceptually, backprojection can be thought of a smearing each profile back across the image in the direction of the radiation propagation. In addition to the filtered backprojection, iterative reconstruction techniques are used. They are often used for the reconstruction with a limited number of projections as described by Lewitt [10] or Huesman [11].

3 EXPERIMENTAL SET-UP

For the present experimental investigations a custom built second generation tomograph with a parallel beam geometry is used (see Figure 3). It is located at the Federal Institute for Materials Research and Testing (BAM) in Berlin. The tomograph consists of a fixed X-ray tube and detector array. The mechanical manipulator translates and rotates the scanned object to obtain the projections. The scanner consists of 15 detectors, which is equal to the number of projections received at a given time. To obtain a 180° scan 12 steps of rotation are made. The spatial resolution is set to 0.4 ×0.4 mm with an imaging time of 15 min. for one image. The source provides a collimated X-ray beam of 40° aperture and 2 mm thickness. The accelerator voltage of the X-ray beam is set to 360 keV with a current of 4 mA. Therefore the energy of the emitted photons is high enough to penetrate the column filled with the ceramic spheres. A filter of 2 mm aluminum and 3 mm copper is attached in front of the X-ray tube to prevent beam hardening effects. Since all substances attenuate low energy X-ray more strongly than high-energy ones, primarily because of photoelectric absorption, a polychromaic beam penetrating an absorbing medium becomes proportionally richer in high energy photons, and hence more penetrating or 'harder' (see Brooks and di Chiro [13] as a reference). The used detectors consist of plastic szintilators attached to photo multipliers. 15 detectors were used, spaced 1° to each other. Therefor 12 rotations steps are necessary to obtain a full set of projections.

The spatial resolution inherent in a CT image depends on two major components, the mechanics of the data-taking and reconstruction of the image as described by Yester and Barnes [14] as well as Glover and Eisner [15]. The reconstruction involves the application of a filter function to a series of object profiles, and an algorithm is used to obtain an image from these profiles. The final image will consists of a matrix of pixels which is the result of the mathematical reconstruction procedure. To decrease the pixel size of the matrix will improve the resolution of the image up to a point. That is the limitation given by the accuracy of the mechanical system and the focal spot of the X-ray beam and aperture of the detectors. The spatial resolution BW (beam width) can approximately be calculated by:

$$BW \cong \frac{\sqrt{d^2 + [a(M-1)]^2}}{M} \quad , \quad M = \frac{L}{q} \tag{3}$$

It is a function of the detector aperture d, the focal spot of the X-ray beam a, the distance between the source and detector L, and the distance between the source and the imaging point q. The focal spot of the X-ray source is a= 0.7 mm and the aperture of the detectors d= 0.5 mm. This results in a resolution of 0.4 mm.

The diameter of the column imaged is 200 mm. The wall of the column is made of acrylic glass with a thickness of 5 mm. The height of the column is 250 mm. As a packing spheres of 10 mm diameter in a random arrangement and a structured Mellapak 250Y form Sulzer are used. The spheres are made of a ceramic material and the structured packing of folded metal with a thickness of 0.1 mm.

For the investigations water is introduced at the top of the column and flows through the respective packing. The liquid distributor consists of a perforated plate with 177 holes of 1 mm diameter. The flow-rates are set so that a stationary flow field is obtained. This can be set for flow-rates of the liquid phase of up to 30 m^3/m^2h. Of the flow inside the packing two-dimensional scans are conducted. The measurement time for one scan is 15 minutes. In order to identify the liquid phase inside the packing, both a dry and a wetted scan are done. The results of both scans are digitally compared to yield the resulting liquid distribution on the elements of the packing. By joining several adjacent two-dimensional scans together a three-dimensional data-set of the measured object is obtained, as depicted in Figure 4 for the structured packing.

4 EXPERIMENTAL RESULTS

In Figure 5 the resulting images of the random packing are displayed. The Figures 5a, and 5b are the results from the reconstruction of the integral measurement values. Those computed linear attenuation coefficients are represented in 256 gray scales. Black corresponds to a small absorption of X-ray (air) and white for a strong one (metal, ceramic).

In Figure 5a the random packing with trickle flow is shown. In Figure 5b the dry random packing is given. In the figure with trickle flow the water is to be recognized in some places already in this representation by comparing it to the figure with the dry packing. To compute Figure 5e the gray scales of Figure 5a have been subtracted from the gray scales in Figure 5b. The resulting image is Figure 5c, which shows the water in the packing only. The distribution of the water in the random packing is clearly visible. To compare the flow of the water with the distribution of the ceramic spheres, the gray scales of Figures 5c and 5d, which represent the packing only, are added to each

other, resulting in the image given in Figure 5e. In this representation it is evident, that the water is distributed very irregularly. There are regions with high liquid holdup and some regions with no water at all. This is due to the randomness of the distribution of the spheres. It is possible that above the depicted plane spheres hinder flowing the water downward through the packing. As a result no water will be observed at the places below. On the other hand the fluid could be obstructed draining by spheres placed below the depicted plane. This results in a high local liquid holdup.

In Figure 6 the local void fraction of the dry random packing is plotted as a function of the relative distance to the wall in dependence of the ratio of the spheres diameter to the diameter of the column. The values of the void fraction calculated out of the measurement values are in good agreement with data given by Brauer [16]. He measured the void fraction by dividing the packed column filled with spheres of cork and wax into slabs and after this into concentric rings. Analysis for void fraction was made by accurately measuring the volume of the slab before and after removal of the annular ring, melting the material removed, and calculating the void volume from the weight of wax and its density. At the wall the local void fraction is one, because the spheres have only infinitesimal small point-contact to the wall. With increasing distance from the wall the local void fraction is more homogenous. The average void fraction of the random packing calculated from the measurements is $\varepsilon = 0.34$. The void fraction given by the manufacture is $\varepsilon = 0.36$, what means a deviation of 5.6 %. In Figure 7 the measurement results for the structured packing is shown, where the dry packing is depicted in Figure 7a and the wet packing is depicted in Figure 7b. The waved structure of the packing surface and the holes in the packing are clearly visible. The random arrangement of the individual metal sheets can be seen. Figure 7c has been calculated in the way described above for the random packing. The liquid film is found all over the elements of the packing, even though the thickness of the liquid layer varies with position of the metal elements. The liquid film on the surfaces with an upward facing normal are about 3 to 4 times thicker than the liquid films on the corresponding reverse surfaces. The liquid film apparently drains from the overhead packing elements to accumulate on the upward facing elements. Where the metal sheets of the packing get close to each other, the water accumulates. This effect can be explained with the surface tension of the liquid phase.

To investigate the axial distribution of the liquid holdup, in Figure 8 the liquid holdup of the random packing averaged over an area of 1 cm^2 is depicted in two planes. The liquid holdup ε_L is calculated from the volume of the liquid phase V_L, the volume of the column V_C and the void fraction ε by

$$\varepsilon_L = \frac{V_L}{V_C \varepsilon}. \tag{4}$$

The resulting distribution for the random spherical packing is correspondingly random. In addition, the pattern of the distribution changes significantly after 2 mm of axial displacement, which is the spatial distance between Figure 8a and b. Therefore, a measurement of the local distribution of the liquid phase is highly dependent on the position inside the column due to the axial inhomogenity of the random packing. In contrast, in the structured packing the liquid distribution is much more homogeneous even in the axial direction. This can be observed by comparing Figure 9a and b, which are also 2 mm apart. Here, the liquid distribution changes only slightly with the axial coordinate, which is in correspondence to the axial structure of the packing. The few zones with a significant higher liquid holdup are located, where two metal sheets of the packing get close to each other and where therefore the water accumulates. The measured and calculated liquid holdups are in good agreement with data given by Suess [17]. He measured the liquid holdup for different structured packings with a gamma ray absorption technique using the water/air system. With the following empirical equation he calculated the liquid holdup within 10% accuracy below the loading point:

$$\varepsilon_L = c a_l^{0.83} l^x \left(\eta_L / \eta_{L,o}\right)^{0.25} \tag{5}$$

where η_L is the dynamic liquid viscosity, $\eta_{L,0}$ the dynamic viscosity of water at 20°C (cP), l the liquid load (m^3/m^2h), and a_l the surface area of the structured packing (for Mellapak Y250 250 m^2/m^3) and

$c = 0.0169$ for $l < 40$ m^3/m^2h,
$c = 0.0075$ for $l > 40$ m^3/m^2h,
$x = 0.37$ for $l < 40$ m^3/m^2h,
$x = 0.59$ for $l > 40$ m^3/m^2h.

The loading point characterizes the condition where liquid holdup increases sharply due to the interaction between gas and liquid phase. The ratio of the dynamic viscosity can be set to one, using water of about 20°C. For the test conditions of a liquid flow rate of 17 m^3/m^2h a liquid holdup of $\varepsilon_L = 4.7\ \%$ is calculated. The measured average liquid-holdup in all planes is about $\bar{\varepsilon}_L = 5\%$.

5 CONCLUSIONS

The experimental results presented in this paper show, that X-ray tomography is applicable for the measurement of the phase distributions of stationary multiphase flows. Due to the high spatial resolutions, even small liquid films on structured packings can be measured. The only disadvantage of the measurement system is the long measurement time, which is reduced when using an X-ray tomograph of third or fourth generation. These tomographs reach measurement times of seconds and less. Regarding the liquid distribution in random packings a very inhomogenous distribution is observed. The changes are drastically in axial direction. This result has to be confirmed be further investigations with other mass-flow-rates. In structured packings the distribution of the liquid phase is more homogenous. The liquid films are thicker on the upward facing side of the metal sheets than on the downward facing side. Maybe this maldistribution is reduced, when a gaseous phase is introduced through the packing in countercurrent flow.

6 ACKNOWLEDGEMENT

The authors wish to thank Dr. J. Goebbels and his team for the help in conducting the experiments as well as Sulzer Chemtech for the supply of different packing material. The financial support of the DFG (Deutsche Forschungsgemeinschaft) is gratefully acknowledged.

7 NOMENCLATURE

a	focal spot of the X-ray source	m
a_l	specific area of packing	m^2/m^3
d	detector aperture	m
f	property distribution	-
L	source-detector distance	m
q	distance source imaging point	m
V_C	volume of the column	m^3
V_L	volume of the liquid phase	m^3
V_P	volume of the packing	m^3
t	time	s
x	coordinate	m
y	coordinate	m
z	coordinate	m
Φ_M	integral measurement value	-
Θ	angel	°
ε	void fraction of packing	$\varepsilon=(V_C-V_P)/V_C$

ε_L	liquid holdup	% of packing
μ	linear attenuation coefficient	1/m
η_L	liquid dynamic viscosity	cP
$\eta_{L,0}$	dynamic viscosity of water at 20°C	cP
ξ	angel	°

8 REFERENCES

[1] G. N. Hounsfield: Computerized transverse axial scanning (tomography): Part I. Description of system, Br. J. Radiology, Vol. 46, 1973, pp. 1016-1022

[2] A. Kantzas: Computation of holdups in fluidized and trickle beds by computer-assisted tomography, AIChE J. Vol. 40, No. 7, 1994, pp. 1254-1261

[3] P.G. Lutran, K.M. Ng, E.P. Delikat: Liquid distribution in trickle beds. An experimental study using computer assisted tomography, Ind. Eng. Chem. Res., Vol. 30, 1991, pp. 1270-1280

[4] D. Toye, P. Marchot, M. Crine, E. L'Homme: The use of large scale computer assisted tomography for the study of hydrodynamics in trickling filters, Chem. Eng. Sc. Vol. 49, No. 24b, 1994, pp. 5271-5280

[5] T. Ikeda, K. Kotani, Y. Meada, H. Kohno: Preliminary study on application of X-ray CT scanner to measurement of void fractions in steady state two-phase flows, J. of Nuclear Science and Technology, Vol. 20, No.1, 1983, pp. 1-12

[6] K. R. Peschmann *et. al.*: High-speed computer tomography: Systems and performance, Applied optics, Vol. 2, No. 23, 1985, pp. 4052-4060

[7] M. M. Ter-Pogossian, M. E. Phelps, G. L. Brownwell *et. al.*: Reconstruction tomography in diagnostic radiology and nuclear medicine, University park press, Baltimore, 1977

[8] G.T. Herman: Image reconstruction from projections the fundamentals of computerized tomography, Academic Press, New York, 1980

[9] R. A. Brooks, G. di Chiro: Principles of computer assisted tomography (CAT) in radiographic an radioisotopic imaging, Phys. Med. Biol., Vol.21, No. 5, 1976, pp. 689-732

[10] A. C. Kak, M. Slaney: Principles of Computed Tomographic Imaging, IEEE Press, New York, 1988

[11] R. M. Lewitt: Processing of incomplete measurement data in computed tomography, Med. Phys. Vol. 6, No. 5, 1979, pp. 412-417

[12] R. H. Huesman: The effects of a finite number of projection angles and finite lateral sampling of projections on the propagation of statistical errors in transverse section Reconstruction, Phys. Med. Biol., Vol. 22, No. 3, 1977, pp. 511-521

[13] R. A. Brooks, G. di Chiro: Beam hardening in X-ray reconstructive tomography, Phys. Med. Biol., Vol. 21, No. 3, 1976, pp. 390-398

[14] M. V. Yester, G. T. Barnes: Geometrical limitations of computed tomography (CT) scanner resolution,Proceedings- Applied optical Instrumentation in Medicine, SPIE, Vol. VI 127, 1977, pp. 296-303

[15] G. H. Glover, R. L. Eisner: Theoretical Resolution of CT Systems, J. of Computer Assisted Tomography, Vol. 3, No. 1, 1979, pp. 85-91

[16] H. Brauer: Grundlagen der Einphasen- und Mehrphasenströmungen, Verlag Sauerländer, Aarau u Frankfurt am Main, 1971

[17] P. Suess L. Spiegel: Holdup of Mellapak structured packings, Chem. Eng. Proc. Vol. 31, 1992, pp. 119-124

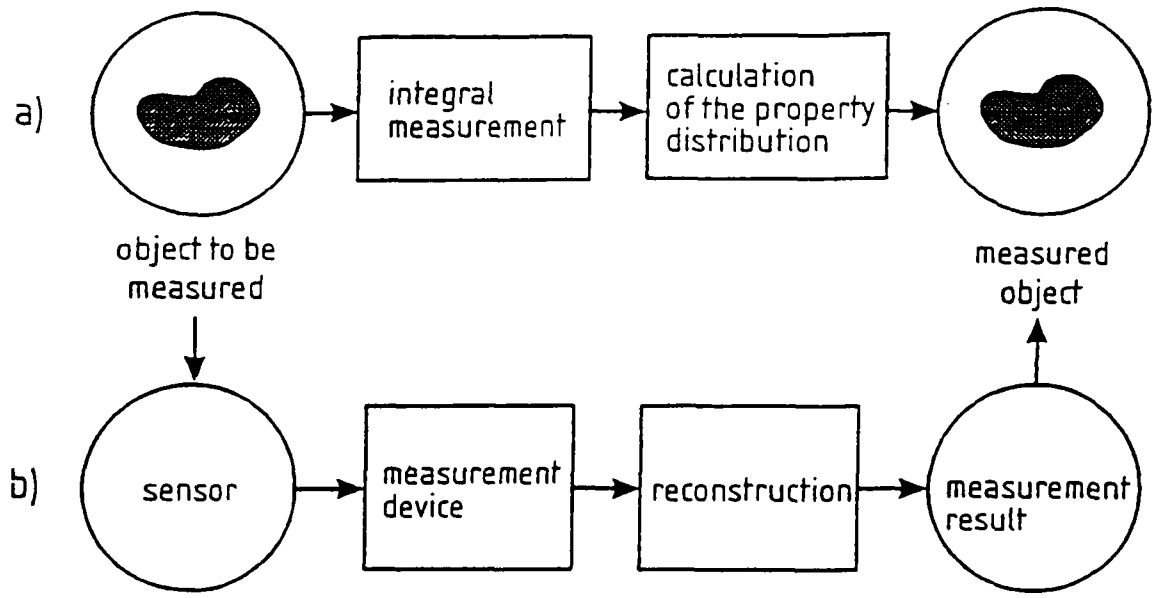

Figure 1: Schematic representation of the imaging principle of tomographic measurement techniques

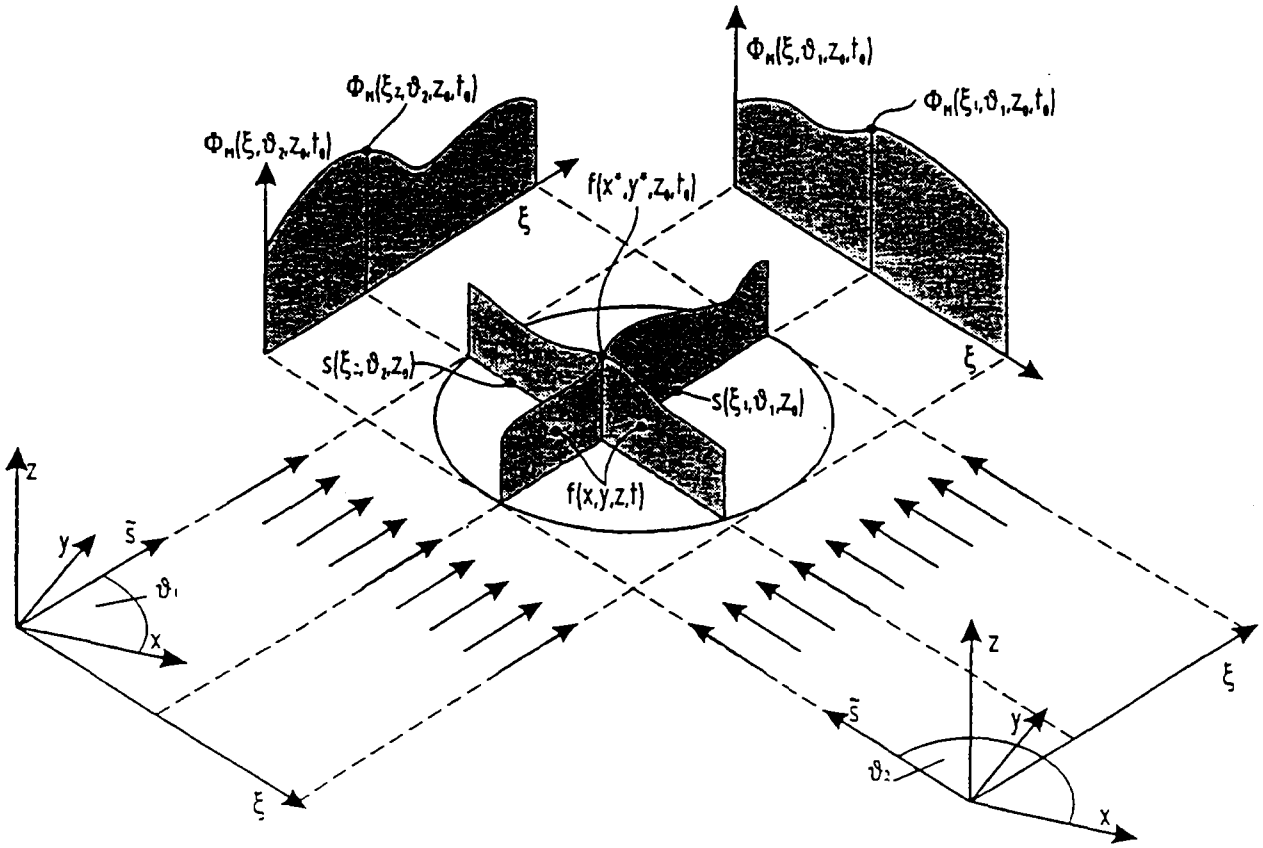

Figure 2: Schematical description of the measurement process

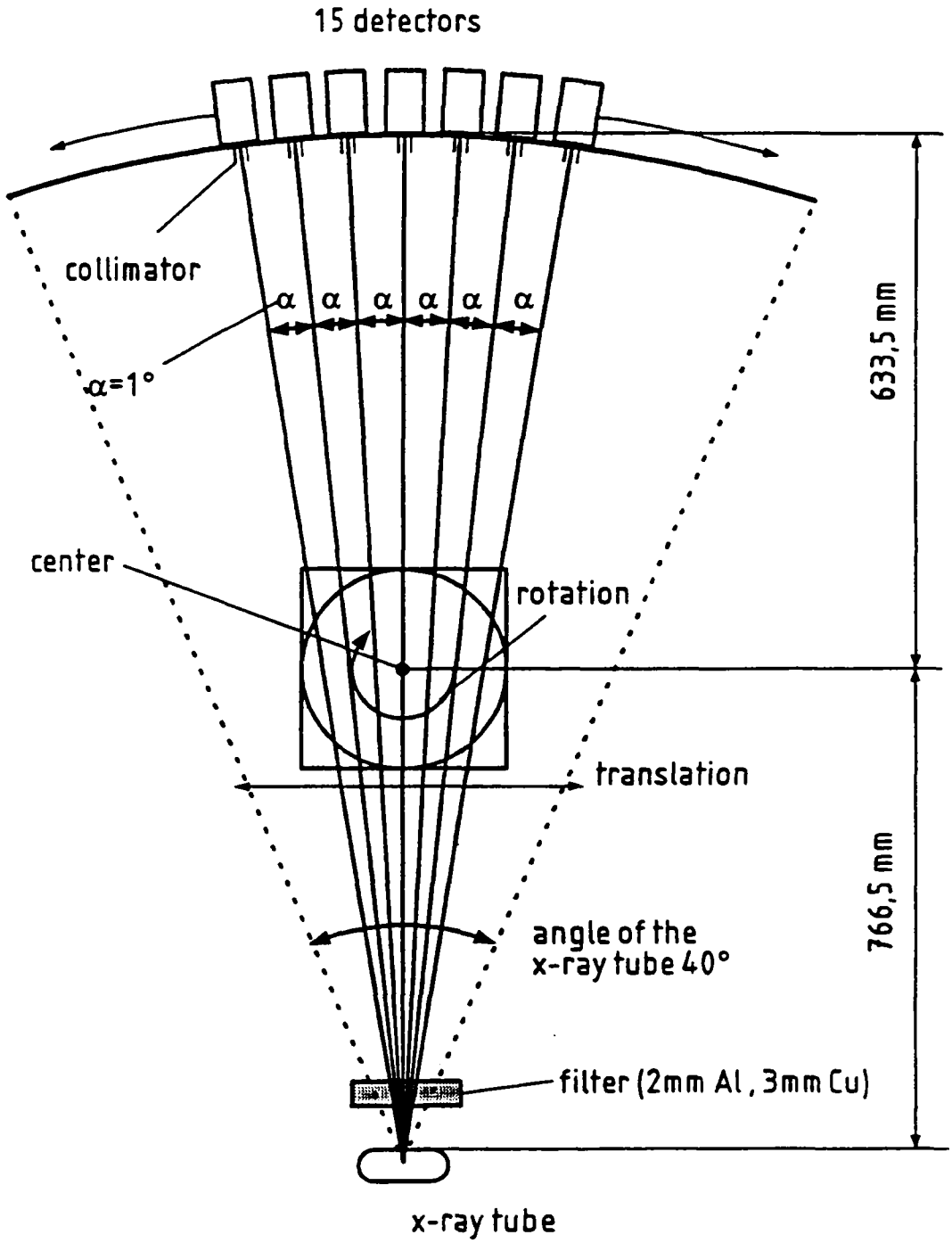

Figure 3: Experimental set-up

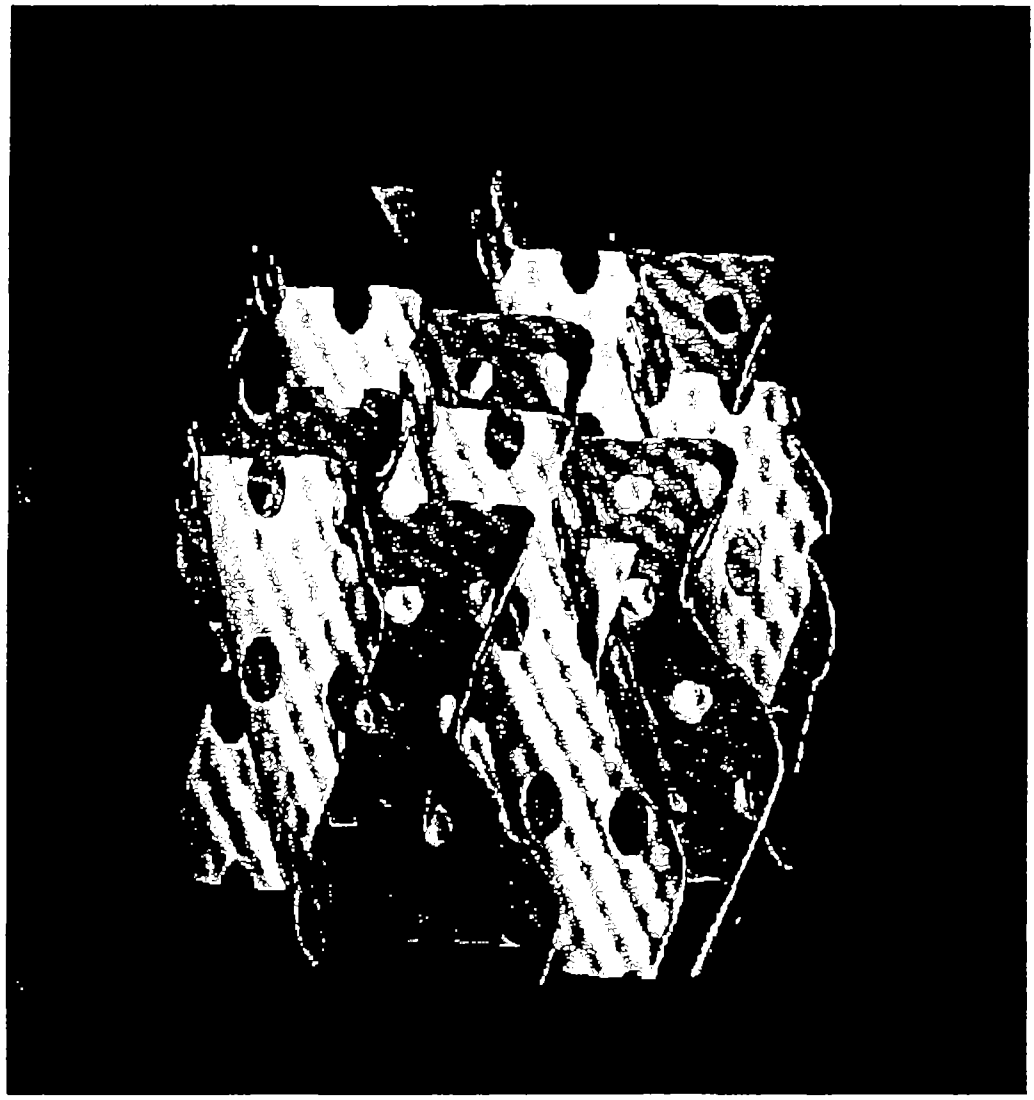

Figure 4: 3-dimensional presentation of the structured packing

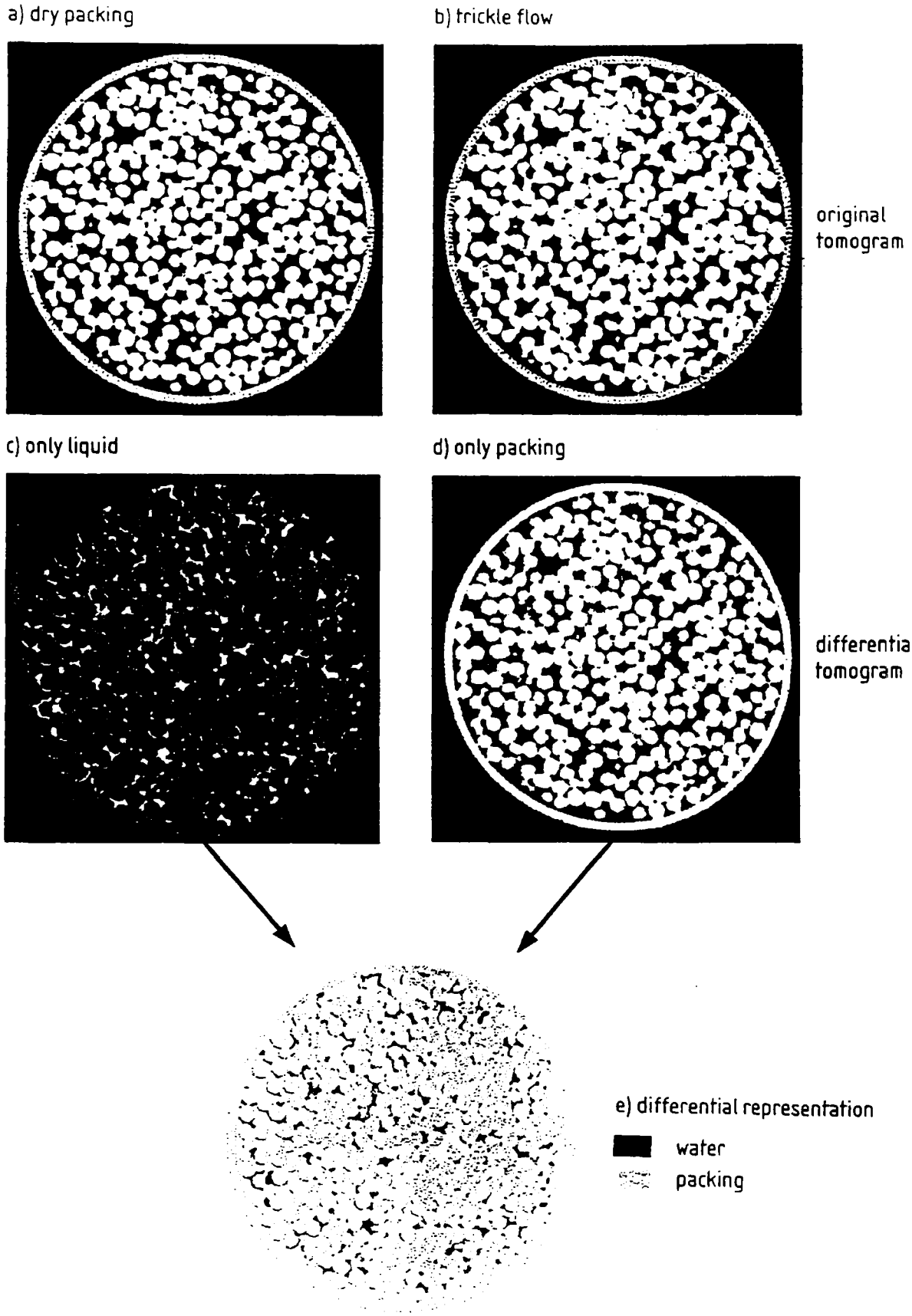

Figure 5: Digitally enhanced tomogram of the random packing

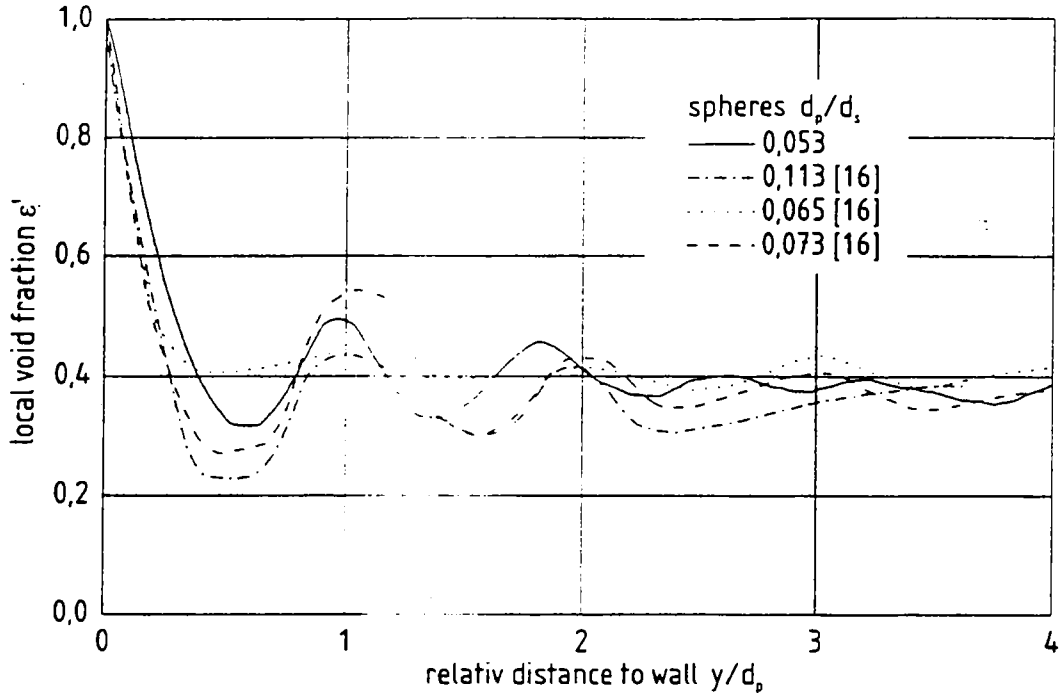

Figure 6: Local void fraction as a function of the relativ distance to wall

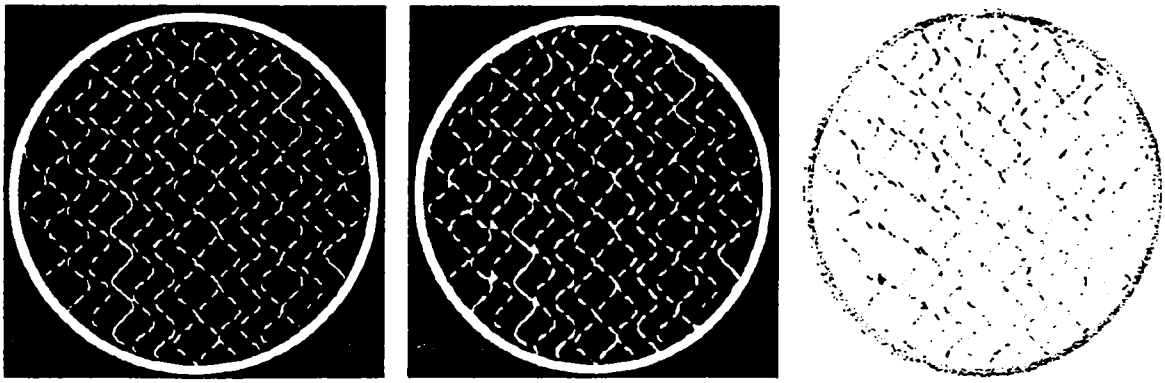

Figure 7: Digitally enhanced tomogram for a structured packing

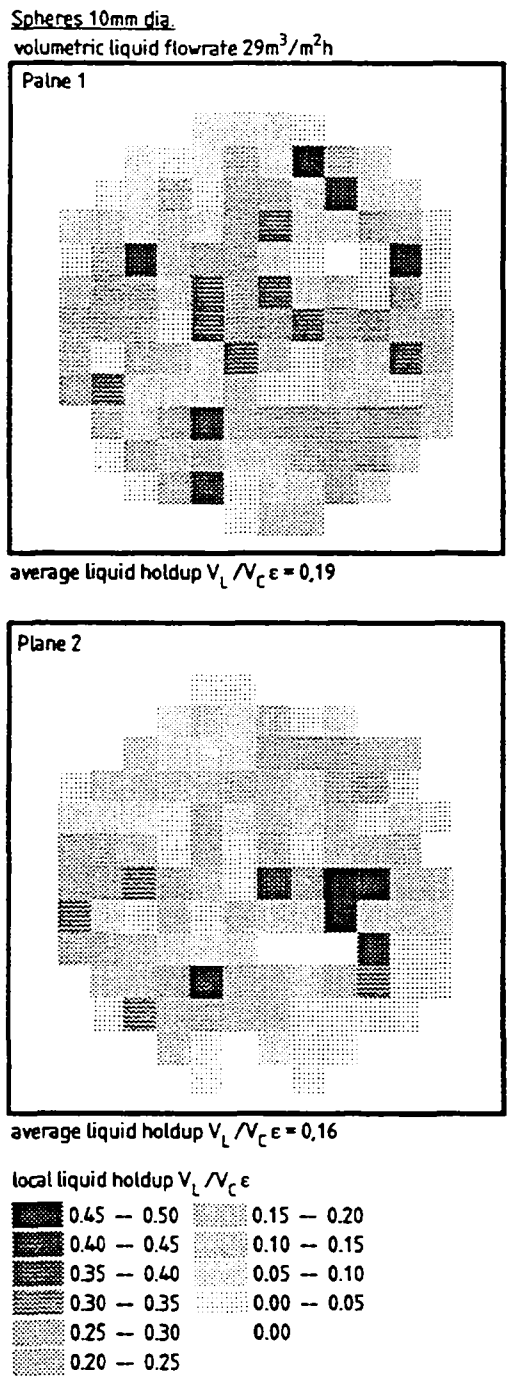

Figure 8: Averaged liquid holdup in the random packing

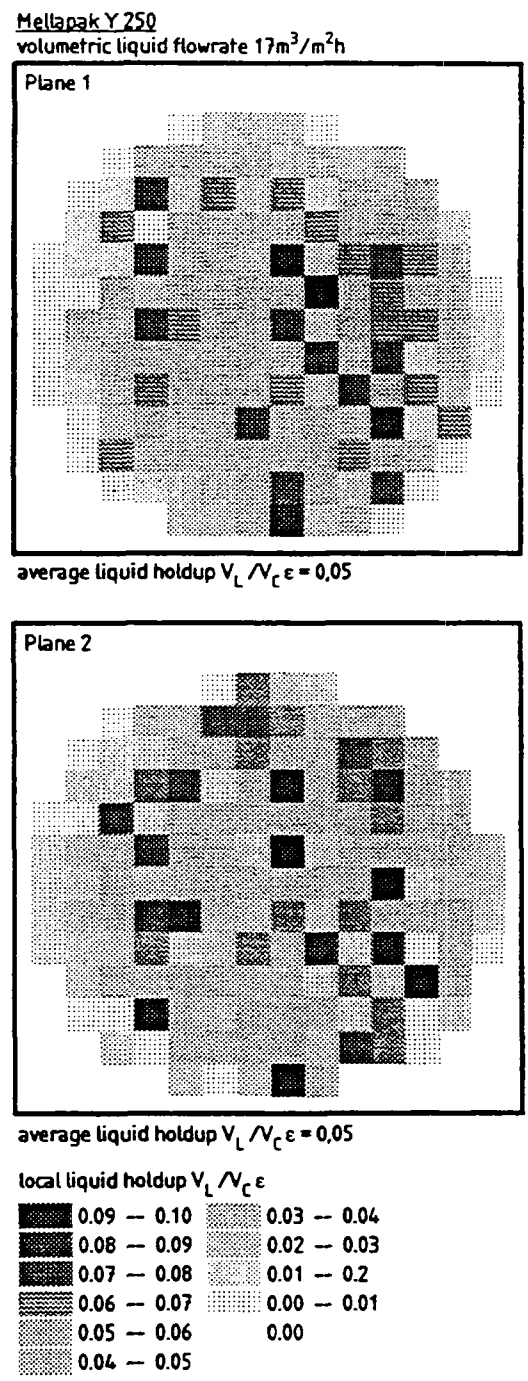

Figure 9: Averaged liquid holdup in the structured packing